

6-15-2017

## Development and Physicochemical Characterization of Acetalated Dextran Aerosol Particle Systems for Deep Lung Delivery

Zimeng Wang  
*University of Rhode Island*

Sweta K. Gupta  
*University of Rhode Island*

Samantha A. Meenach  
*University of Rhode Island, smeenach@uri.edu*

Follow this and additional works at: [https://digitalcommons.uri.edu/che\\_facpubs](https://digitalcommons.uri.edu/che_facpubs)

 Part of the [Chemical Engineering Commons](#)

---

### Citation/Publisher Attribution

Wang, Z., Gupta, S. K., & Meenach, S. (2017). Development and Physicochemical Characterization of Acetalated Dextran Aerosol Particle Systems for Deep Lung Delivery. *International Journal of Pharmaceutics*, 525(1), 264-274. doi:10.1016/j.ijpharm.2017.04.052  
Available at: <http://dx.doi.org/10.1016/j.ijpharm.2017.04.052>

This Article is brought to you by the University of Rhode Island. It has been accepted for inclusion in Chemical Engineering Faculty Publications by an authorized administrator of DigitalCommons@URI. For more information, please contact [digitalcommons-group@uri.edu](mailto:digitalcommons-group@uri.edu). For permission to reuse copyrighted content, contact the author directly.

---

# Development and Physicochemical Characterization of Acetalated Dextran Aerosol Particle Systems for Deep Lung Delivery

## Disciplines

Chemical Engineering

The University of Rhode Island Faculty have made this article openly available.  
Please let us know how Open Access to this research benefits you.

This is a pre-publication author manuscript of the final, published article.

## Terms of Use

This article is made available under the terms and conditions applicable towards Open Access Policy Articles, as set forth in our [Terms of Use](#).

1 **Development and Physicochemical Characterization of Acetalated Dextran Aerosol**  
2 **Particle Systems for Deep Lung Delivery**

3  
4 Zimeng Wang<sup>1</sup>, Sweta K. Gupta<sup>1</sup>, Samantha A. Meenach<sup>1,2</sup>  
5  
6

7  
8 <sup>1</sup>University of Rhode Island, College of Engineering, Department of Chemical  
9 Engineering, Kingston, RI 02881, USA

10  
11 <sup>2</sup>University of Rhode Island, College of Pharmacy, Department of Biomedical and  
12 Pharmaceutical Sciences, Kingston, RI 02881, USA  
13

14  
15  
16  
17 **Corresponding Author:** Samantha A. Meenach, University of Rhode Island, 205  
18 Crawford Hall, 16 Greenhouse Road, Kingston, RI, 02881, USA. Email:  
19 smeenach@uri.edu  
20  
21

33 **ABSTRACT**

34 Biocompatible, biodegradable polymers are commonly used as excipients to  
35 improve the drug delivery properties of aerosol formulations, in which acetalated dextran  
36 (Ac-Dex) exhibits promising potential as a polymer in various therapeutic applications.  
37 Despite this promise, there is no comprehensive study on the use of Ac-Dex as an  
38 excipient for dry powder aerosol formulations. In this study, we developed and  
39 characterized pulmonary drug delivery aerosol microparticle systems based on spray-  
40 dried Ac-Dex with capabilities of (1) delivering therapeutics to the deep lung, (2)  
41 targeting the particles to a desired location within the lungs, and (3) releasing the  
42 therapeutics in a controlled fashion. Two types of Ac-Dex, with either rapid or slow  
43 degradation rates, were synthesized. Nanocomposite microparticle (nCmP) and  
44 microparticle (MP) systems were successfully formulated using both kinds of Ac-Dex as  
45 excipients and curcumin as a model drug. The resulting MP were collapsed spheres  
46 approximately 1  $\mu\text{m}$  in diameter, while the nCmP were similar in size with wrinkled  
47 surfaces, and these systems dissociated into 200 nm nanoparticles upon reconstitution in  
48 water. The drug release rates of the Ac-Dex particles were tuned by modifying the  
49 particle size and ratio of fast to slow degrading Ac-Dex. The pH of the environment was  
50 also a significant factor that influenced the drug release rate. All nCmP and MP systems  
51 exhibited desirable aerodynamic diameters that are suitable for deep lung delivery (e.g.  
52 below 5  $\mu\text{m}$ ). Overall, the engineered Ac-Dex aerosol particle systems have the potential  
53 to provide targeted and effective delivery of therapeutics into the deep lung.

54

55 **KEYWORDS:** Acetalated dextran, nanocomposite microparticles, microparticles,  
56 pulmonary delivery, spray drying, controlled release

57

## 58 **1. INTRODUCTION**

59 Pulmonary drug delivery has exhibited promising potential in the treatment of  
60 lung diseases, as it allows for the delivery of a wide range of therapeutics directly and  
61 efficiently to the lungs, thereby increasing local drug concentration, reducing systemic  
62 side effects, providing a rapid onset of pharmaceutical action, and avoiding the first-pass  
63 metabolism associated with the liver (Belotti et al., 2015; Cui et al., 2011; Mansour et al.,  
64 2009; Meenach et al., 2012). The deep lung (alveolar) region can be utilized as a route  
65 for systematic drug delivery due to the enormous surface area available and nearby  
66 plentiful capillary vessels that facilitate drug absorption, the very thin (approximately 0.1  
67  $\mu\text{m}$ ) liquid layer over the alveoli that ensures rapid and unhindered drug absorption, and  
68 low enzymatic activity, which enhances drug availability (Collier et al., 2016; Cui et al.,  
69 2011; Hoang et al., 2014). As a result, various therapeutics such as antibiotics, proteins,  
70 peptides, anti-cancer drugs (Wu et al., 2014), plasmid DNA (Takashima et al., 2007),  
71 siRNA (Jensen et al., 2010), and anti-tuberculosis (TB) drugs have been employed in  
72 inhalation formulations for the treatment of pulmonary diseases such as asthma, chronic  
73 obstructive pulmonary disease (COPD), cystic fibrosis (CF)-related pulmonary  
74 infections, and lung cancer (Meenach et al., 2013a; Wu et al., 2014).

75 Dry powders are a dosage formulation that delivers therapeutics to the lung, in the  
76 form of particles, using a dry powder inhaler (Wu et al., 2014). Compared with liquid  
77 aerosols, these formulations offer additional benefits such as enhanced stability of the

78 formulation, controllable particle size for targeting different regions of the lung, and  
79 increased drug loading of hydrophobic payloads (Cohen et al., 2010; Meenach et al.,  
80 2013a). Spray drying has proven to be a suitable technology in the preparation of dry  
81 powder therapeutics (Meenach et al., 2013a), as it is capable of producing respirable  
82 microparticles for deep lung delivery with acceptable aerosol dispersion properties  
83 (Belotti et al., 2015). Properties of dry powder particles such as particle size, particle  
84 shape, and surface morphology can be modified by controlling the spray drying  
85 production process, thus providing desirable particle characteristics (Belotti et al., 2015;  
86 Wu et al., 2014).

87 Biocompatible, biodegradable polymers such as poly( $\epsilon$ -caprolactone) (PCL) and  
88 poly(lactic-co-glycolic acid) (PLGA) have been used as dry powder formulation  
89 excipients to carry drug molecules, protect drugs from degradation, and impart sustained  
90 release to aerosol formulations (Mansour et al., 2009). However, PLGA and PCL  
91 delivery systems show significant burst release of their payloads due to bulk erosion of  
92 the polymers and it is difficult to control the polymer degradation rate and modulate their  
93 release profiles (Ulery et al., 2011). Acetalated dextran (Ac-Dex) is an acid-sensitive,  
94 biodegradable, biocompatible polymer prepared via a one-step reaction by reversibly  
95 modifying dextran with acetal groups. This modification reverses the solubility properties  
96 of dextran from hydrophilic to hydrophobic, making it possible to form polymeric  
97 particles using standard emulsion or nanoprecipitation techniques. In contrast to other  
98 commonly used polymers such as PLGA, polylactic acid, and PCL, Ac-Dex exhibits  
99 attractive properties suitable for the controlled release of therapeutic payloads. By  
100 controlling the reaction time during the formation of Ac-Dex, the ratio of cyclic acetal

101 groups (with a slower degradation rate) to acyclic acetal groups (with a faster degradation  
102 rate) can be adjusted. As a result, the degradation rate of the resulting Ac-Dex can be  
103 tuned from hours to months to suit various applications. Moreover, the acid-sensitivity of  
104 Ac-Dex enables it to degrade faster in lower pH environments, such as lysosomes in  
105 macrophage or tumor cells, allowing for controlled release of drug within these cells.  
106 Furthermore, Ac-Dex degrades into neutral by-products, which avoids undesirable  
107 changes in the micro-environmental pH in the body. Finally, Ac-Dex offers the potential  
108 of targeted delivery, due to the presence of dextran chains that can be further modified  
109 with a variety of functional targeting moieties (Bachelder et al., 2008; Broaders et al.,  
110 2009; Kauffman et al., 2012).

111 Owing to the aforementioned advantages, Ac-Dex has been widely applied in the  
112 formation of polymeric carriers for drug delivery. Porous Ac-Dex microparticles loaded  
113 with the chemotherapeutic camptothecin were developed for pulmonary delivery using  
114 emulsion techniques. These systems exhibited a respirable fraction of 37% and  
115 experimental mass mean aerodynamic diameters from 5.3 - 11.9  $\mu\text{m}$  (Meenach et al.,  
116 2012). Ac-Dex nanoparticle systems have been investigated in the application of protein  
117 delivery for immunotherapy (Broaders et al., 2009), gene delivery to phagocytic and non-  
118 phagocytic cells (Cohen et al., 2010), tandem delivery of peptide and chemotherapeutic  
119 for controlled combination chemotherapy (Cui et al., 2011), delivery of the host-mediated  
120 compound AR-12 (Arno Therapeutics; formerly known as OSU-03012) for the treatment  
121 of *Leishmania donovani* (Collier et al., 2016), and the control of *Salmonella* infections  
122 (Collier et al., 2016). Both Ac-Dex nanoparticles and microparticles loaded with

123 horseradish peroxidase have been evaluated to improve vaccine stability outside cold  
124 chain conditions (Kanthamneni et al., 2012).

125 Despite this work, there is no comprehensive study on using Ac-Dex as an  
126 excipient for dry powder aerosol formulations produced via spray drying. In this study,  
127 we aimed to develop and characterize dry powder pulmonary delivery systems based on  
128 spray-dried Ac-Dex particles with capabilities of (a) delivering therapeutics to the deep  
129 lung, (b) targeting the particles to a particular location within the lungs, and (c) releasing  
130 therapeutics at a controlled rate. Previous studies have shown that: (a) aerodynamic  
131 diameter ( $d_a$ ) determines the region of the lungs where particles will deposit, where  
132 particles with an  $d_a$  of 1 - 5  $\mu\text{m}$  tend to deposit in the deep lung region (Meenach et al.,  
133 2013a); (b) geometric size plays an important role in the cellular uptake of particles,  
134 where nanoscale particles (approximately 150 nm) tend to escape phagocytic uptake (He  
135 et al., 2010), while particles larger than 1  $\mu\text{m}$  will suffer from macrophage clearance in  
136 the alveoli (Kho et al., 2010); and (c) the drug release rate of Ac-Dex particles can be  
137 tuned by modifying the synthesis time of the Ac-Dex polymer (Kauffman et al., 2012;  
138 Meenach et al., 2012).

139 To prepare the engineered particle systems, two types of Ac-Dex with rapid or  
140 slow degradation rates were synthesized. Nanocomposite microparticle (nCmP) and  
141 microparticle (MP) systems were formulated using both kinds of Ac-Dex as the  
142 excipient. Curcumin was used as model drug owing to its high hydrophobicity (similar to  
143 many other pulmonary therapeutics) and fluorescence (allowing for easy detection). The  
144 nCmP were prepared by spray drying an aqueous suspension of CUR-loaded Ac-Dex  
145 nanoparticles (NP, 200 nm) and the solid MP were formulated by spray drying a solution



146 of Ac-Dex and CUR in a solution of tetrahydrofuran (THF) and acetone. We hypothesize  
147 that upon pulmonary administration, the nCmP will deposit in the deep lung, decompose  
148 into free NP, and facilitate the sustained release of drug to the targeted site, while the MP  
149 will remain the original size after deposition in the deep lung region. A schematic of the  
150 described particle preparation and design is shown in **Figure 1**. Overall, the goal of the  
151 described research was the initial development and physicochemical characterization of  
152 dry powder Ac-Dex aerosol particle systems with the potential for effective delivery of  
153 therapeutics.

154

## 155 **2. MATERIALS AND METHODS**

156

### 157 **2.1 Materials**

158 Dextran from *Leuconostoc mesenteroides* (9000-11000 MW), pyridinium p-  
159 toluenesulfonate (PPTS, 98%), 2-methoxypropene (2-MOP, 97%), triethylamine (TEA,  $\geq$   
160 99%), anhydrous dimethyl sulfoxide (DMSO,  $\geq$  99.9%), poly(vinyl alcohol) (PVA, MW  
161 13,000-23,000, 87-89% hydrolyzed), dichloromethane (DCM, anhydrous,  $\geq$  99.8%),  
162 deuterium chloride (DCl, 35 weight % in D<sub>2</sub>O, 99 atom % D), Tween<sup>®</sup> 80, curcumin,  
163 sodium acetate ( $\geq$  99%), acetic acid solution (1.0 N), acetone ( $\geq$  99.8%), tetrahydrofuran  
164 (THF,  $\geq$  99%), and methanol (anhydrous,  $\geq$  99.9%) were obtained from Sigma–Aldrich  
165 (St. Louis, MO). Deuterium oxide (D<sub>2</sub>O, 99.8% atom D) was obtained from Acros  
166 Organics (Geel, Belgium). Phosphate buffered saline (PBS) was obtained from Fisher  
167 Scientific (Somerville, NJ). Hydranal<sup>®</sup> KF reagent was obtained from Fluka Analytical.

168

## 169 **2.2 Synthesis and NMR Analysis of Acetalated Dextran (Ac-Dex)**

170 Ac-Dex was synthesized as described previously (Bachelder et al., 2008) with  
171 minor modifications. 1 g of lyophilized dextran and 25 mg of PPTS were dissolved in 10  
172 mL of anhydrous DMSO. The resulting solution was reacted with 5 mL of 2-MOP under  
173 nitrogen gas for 5 minutes to prepare Ac-Dex with a rapid degradation rate (Ac-Dex-  
174 5min) or for 3 hours to prepare Ac-Dex with a slower degradation rate (Ac-Dex-3h). The  
175 reaction was quenched with 1 mL of TEA. The reaction mixture was then precipitated in  
176 basic water (water and TEA, pH 9), vacuum filtered, and lyophilized ( $-50\text{ }^{\circ}\text{C}$ , 0.023  
177 mbar) for 24 hours to yield a solid product.

178 The cyclic-to-acyclic (CAC) ratio of acetal coverage and degrees of total acetal  
179 coverage per 100 glucose molecules was confirmed by  $^1\text{H}$  NMR spectroscopy (Bruker  
180 300 MHz NMR, MA). 10 mg of Ac-Dex was added to 700  $\mu\text{L}$  of  $\text{D}_2\text{O}$  and was  
181 hydrolyzed with 30  $\mu\text{L}$  of DCl prior to analysis. The hydrolysis of one cyclic acetal group  
182 produces one acetone molecule whereas one acyclic acetal produces one acetone and one  
183 methanol molecule each. Consequently, from the normalized integration of peaks related  
184 to acetone, methanol, and the carbon ring of dextran, the CAC ratio of acetal coverage  
185 and degrees of total acetal coverage per 100 glucoses were determined.

186

## 187 **2.3 Formation of CUR-Loaded Ac-Dex Nanoparticles (CUR NP)**

188 Curcumin-loaded nanoparticles (CUR NP) were prepared via an oil/water  
189 emulsion solvent evaporation using Ac-Dex-5min, Ac-Dex-3h, or a mixture of both types  
190 of Ac-Dex (50 % w/w). 49 mg of Ac-Dex and 1 mg of CUR were dissolved in 1 mL of  
191 DCM over an ice bath, establishing the organic phase. The aqueous phase was comprised

192 of 6 mL of 3% PVA in PBS and was added to the organic phase. The resulting mixture  
193 was sonicated (Q500 Sonicator, Qsonica, Newtown, CT) for 30 seconds with a 1 second  
194 on/off pulse at 70% amplitude. The emulsion was transferred to a spinning solution of  
195 0.3% PVA in PBS and was stirred for 3 hours to allow for evaporation of the organic  
196 solvent and particle hardening. The solution was then centrifuged at 19802 ×g for 20  
197 minutes to collect the nanoparticles. Nanoparticles were washed once with DI water,  
198 redispersed in 0.1% PVA, and lyophilized (−50 °C, 0.023 mbar) for 48 hours. The  
199 resulting NP systems were: CUR NP-5min (made of Ac-Dex-5min only), CUR NP-3h  
200 (made of Ac-Dex-3h only), and CUR NP-h (50 wt% Ac-Dex-5min and 50 wt% Ac-Dex-  
201 3h).

202

#### 203 **2.4 Formulation of CUR Nanocomposite Microparticles (CUR nCmP) via Spray** 204 **Drying**

205 CUR nCmP were prepared via the spray drying of an aqueous suspension of each  
206 type of CUR NP (0.5%, w/v) using a Büchi B-290 spray dryer (Büchi Labortechnik, AG,  
207 Switzerland) in open mode. The CUR NP suspension was sonicated for 10 minutes  
208 before spray drying. The spray drying conditions were as follows: inlet temperature of 60  
209 °C (outlet temperature of  $32 \pm 2$  °C), 0.7 mm nozzle diameter, atomization gas flow rate  
210 of 414 L/h using dry nitrogen, aspiration rate of 28 m<sup>3</sup>/h, pump rate of 0.9 mL/min, and  
211 nozzle cleaner rate of 3. The resulting nCmP were separated in a high-performance  
212 cyclone, dried for 15 minutes in the spray dryer for further removal of residual water,  
213 collected in a sample collector, and stored in amber glass vials in a desiccator at −20°C.

214 nCmP comprised of each kind of NP described previously were produced: nCmP-5min,  
215 nCmP-3h, and nCmP-h, correspondingly.

216

## 217 **2.5 Formulation of CUR Microparticles (CUR MP) via Spray Drying**

218 Solid curcumin-loaded microparticles (CUR MP) were prepared via the spray  
219 drying of an organic solution comprised of Ac-Dex and CUR using a Büchi B-290 spray  
220 dryer in closed mode. The organic solutions were prepared by dissolving CUR and Ac-  
221 Dex (2:98 w/w) in an organic solvent comprised of 85% acetone and 15% THF (v/v) at a  
222 solids concentration of 2% (w/v). The spray drying conditions were as follows: inlet  
223 temperature of 60 °C (outlet temperature of  $40 \pm 2$  °C), 0.7 mm nozzle diameter,  
224 atomization gas flow rate of 414 L/h using UHP dry nitrogen, aspiration rate of 40 m<sup>3</sup>/h,  
225 pump rate of 3 mL/min, and nozzle cleaner rate of 0. The resulting MP were separated in  
226 a high-performance cyclone, dried for 15 minutes in the spray dryer for further removal  
227 of residual solvent, collected in a sample collector, and stored in amber glass vials in a  
228 desiccator at -20°C. The resulting MP were: MP-5min (from Ac-Dex-5min), MP-3h  
229 (from Ac-Dex-3h), and MP-h (from 50 wt% Ac-Dex-5min and 50 wt% Ac-Dex-3h).

230

## 231 **2.6 Particle Size, Size Distribution, and Zeta Potential Analysis**

232 The average diameter, size distribution, and zeta potential of the original NP and  
233 the NP released from the dispersion of nCmP in water were measured by dynamic light  
234 scattering (DLS) using a Malvern Nano Zetasizer (Malvern Instruments, Worcestershire,  
235 UK). The original NP and nCmP were dispersed in DI water (pH = 7, 0.3 mg/mL) prior

236 to analysis. All experiments were performed in triplicate with a scattering angle of  $173^\circ$   
237 at  $25^\circ\text{C}$ .

238

## 239 **2.7 Particle Morphology and Shape Analysis via Scanning Electron Microscopy** 240 **(SEM)**

241 The shape and surface morphology of the nCmP and MP were evaluated by SEM  
242 using a Zeiss SIGMA VP Field Emission-Scanning Electron Microscope (FE-SEM)  
243 (Germany). Particle samples were placed on aluminum SEM stubs (Ted Pella, Inc.,  
244 Redding, CA) with double-sided adhesive carbon tabs. The samples were coated with a  
245 thin film of a gold/palladium alloy using a BIO-RAD sputter coating system at  $20\ \mu\text{A}$  for  
246 60 seconds under argon gas. Images were captured at 8 kV at various magnifications. The  
247 geometric mean diameter and standard deviation of the MP were measured digitally from  
248 SEM images using ImageJ software (Rasband, 1997-2016). Representative micrographs  
249 (5000x magnification) for each sample were analyzed by measuring the diameter of at  
250 least 300 particles.

251

## 252 **2.8 Tapped Density Evaluation of nCmP and MP**

253 The tapped density of the particles was measured as described previously with  
254 minor modifications (Tomoda et al., 2008). 35 - 40 mg of particles was weighed into a  
255 glass tube. The tube was tapped 200 times to ensure efficient packing of the particles and  
256 then the volume occupied by the particles was measured using calipers. The density of  
257 the particles was then determined by the following equation:

258

259  $\rho = \frac{m}{V}$  (1)

260

261 where  $\rho$  is the tapped density,  $m$  is the particle mass, and  $V$  is the volume occupied by the  
262 particles as determined by measuring the height of the particles in the tube with a known  
263 diameter (5 mm). The theoretical mass median aerodynamic diameter ( $MMAD_T$ ) of the  
264 particles was then calculated using the following equation:

265

266  $MMAD_T = d \sqrt{\frac{\rho}{\rho^*}}$  (2)

267

268 where  $d$  is the geometric diameter determined by ImageJ,  $\rho$  is the tapped density of the  
269 particles, and  $\rho^* = 1 \text{ g/cm}^3$ , which is the reference density of solid polymer.

270

## 271 **2.9 Drug Loading Analysis of nCmP and MP**

272 The drug loading and encapsulation efficiency of CUR nCmP and CUR MP were  
273 determined via fluorescence spectroscopy (Biotek Cytation 3, Winooski, VT). All  
274 particle samples were dissolved in DMSO and were evaluated at 420 nm (excitation) and  
275 520 nm (emission). The CUR drug loading and encapsulation efficiency (EE) of the  
276 particles were determined by the following equations:

277

Drug loading =  $\frac{\text{mass of CUR loaded in particles}}{\text{mass of particles}}$  (3)

278

Encapsulation efficiency (EE) =  $\frac{\text{mass of CUR loaded in particles}}{\text{initial mass of CUR in particles}} \times 100\%$  (4)

279

## 280 **2.10 *In Vitro* Drug Release from nCmP and MP**

281 The *in vitro* release profiles of CUR from nCmP and MP were determined via the  
282 release of suspended particles (0.5 mg/mL, 1.5 mL) in modified phosphate buffer (0.1 M,  
283 pH = 7.4, 0.5 wt% Tween<sup>®</sup> 80) and modified acetate buffer (0.1 M, pH = 5, 0.5 wt%  
284 Tween<sup>®</sup> 80). The particle suspensions were incubated at 37 °C and 100 rpm (Digital Heat  
285 Block and ORBi shaker, Benchmark Scientific, Edison, NJ). At various time points,  
286 particle samples were centrifuged at 23102 ×g for 5 minutes at 4 °C to isolate the NP.  
287 200 µL of supernatant was withdrawn and replaced by the same amount of fresh modified  
288 buffer in each sample. The withdrawn solutions were mixed with an equal volume of  
289 DMSO and analyzed for CUR content via fluorescence spectroscopy using the same  
290 method described for drug loading. The release data was fitted to several commonly  
291 utilized drug release models (Supplemental Information **Section S.1**) to elucidate the  
292 mechanism of drug release of Ac-Dex particles. The coefficient of determination ( $R^2$ )  
293 was applied to test the applicability of the described release models.

294

## 295 **2.11 Differential Scanning Calorimetry (DSC)**

296 The thermal phase transitions of nCmP, MP, and their raw components were  
297 determined via DSC using a TA Q10 DSC system (TA Instruments, New Castle, DE,  
298 USA) equipped with an automated computer-controlled TA instruments DSC refrigerated  
299 cooling system. 1 - 3 mg of sample was weighed into Tzero™ alodine-coated aluminum  
300 pans that were hermetically sealed. The sealed pans were placed into the DSC furnace

301 along with an empty sealed reference pan. The heating range was 0 – 200 °C at a heating  
302 rate of 10 °C/min.

303

### 304 **2.12 Powder X-Ray Diffraction (PXRD)**

305 The crystalline states of nCmP, MP, and its raw components were examined by  
306 PXRD using a Rigaku Multiflex X-ray diffractometer (The Woodlands, TX) with a Cu  
307 K $\alpha$  radiation source (40 kV, 44 mA). The samples were placed on a horizontal quartz  
308 glass sample holder (3 mm) prior to analysis. The scan range was 5 – 60° in 2 $\Theta$  with a  
309 step width of 0.1 and scan rate of 1 °/min.

310

### 311 **2.13 Karl Fischer Coulometric Titration**

312 The water content of nCmP and MP was quantified by Karl Fischer (KF) titration  
313 using a 737 KF coulometer (Metrohm, Riverview, FL). 5 mg of powder was dissolved in  
314 anhydrous methanol. The resulting solution was injected into the KF reaction cell filled  
315 with Hydranal<sup>®</sup> KF reagent and then the amount of water was analyzed. Pure solvent was  
316 also injected for use as a background sample.

317

### 318 **2.14 *In Vitro* Aerosol Dispersion Performance with the Next Generation Impactor** 319 **(NGI)**

320 *In vitro* aerosol dispersion performance of nCmP and MP was evaluated using a  
321 Next Generation Impactor<sup>™</sup> (NGI<sup>™</sup>, MSP Corporation, Shoreview, MN) equipped with  
322 a stainless steel induction port (USP throat adaptor) attachment and stainless steel  
323 gravimetric insert cups. The NGI<sup>™</sup> was coupled with a Copley TPK 2000 critical flow



324 controller, which was connected to a Copley HCP5 vacuum pump (Copley Scientific,  
325 United Kingdom). The air flow rate (Q) was measured and adjusted to 60 L/min before  
326 each experiment in order to model the flow rate in a healthy adult lung. Glass fiber filters  
327 (55 mm, Type A/E, Pall Life Sciences, PA) were placed in the gravimetric insert cups for  
328 stages 1 through 7 to minimize particle bounce or re-entrapment (Meenach et al., 2013a)  
329 and these filters were weighed before and after the experiment to determine the particle  
330 mass deposited on each stage. Approximately 10 mg of powder was loaded into a  
331 hydroxypropyl methylcellulose (HPMC, size 3, Quali-V<sup>®</sup>, Qualicaps<sup>®</sup> Inc., Whitsett, NC,  
332 USA) capsule and the capsule was placed into a human dry powder inhaler device  
333 (HandiHaler, Boehringer Ingelheim Pharmaceuticals, CT) attached to a customized  
334 rubber mouthpiece connected to the NGI<sup>™</sup>. Three HPMC capsules were loaded and  
335 released in each measurement and experiments were performed in triplicate. The NGI<sup>™</sup>  
336 was run with a delay time of 10 s and running time of 10 s. For Q = 60 L/min, the  
337 effective cutoff diameters for each stage of the impactor were given from the  
338 manufacturer as: stage 1 (8.06  $\mu\text{m}$ ); stage 2 (4.46  $\mu\text{m}$ ); stage 3 (2.82  $\mu\text{m}$ ); stage 4 (1.66  
339  $\mu\text{m}$ ); stage 5 (0.94  $\mu\text{m}$ ); stage 6 (0.55  $\mu\text{m}$ ); and stage 7 (0.34  $\mu\text{m}$ ). Our previous study on  
340 the relationship between particle mass distribution and payload distribution showed that  
341 no significant difference existed between the drug amount and particle mass in each  
342 chamber of NGI ( $p > 0.05$ ), indicating that the drug was uniformly dispersed in both  
343 CUR-MP and CUR-nCmP (**Figure S1**). The fine particle fraction (FPF), respirable  
344 fraction (RF), and emitted dose (ED) were calculated as follows:

$$\text{Fine particle fraction (FPF)} = \frac{\text{mass of particles on Stages 2 through 7}}{\text{initial particle mass loaded into capsules}} \times 100\% \quad (5)$$

345

$$\text{Respirable fraction (RF)} = \frac{\text{mass of particles on Stages 2 through 7}}{\text{total particle mass on all stages}} \times 100\% \quad (6)$$

$$\text{Emitted dose (ED)} = \frac{\text{initial mass in capsules} - \text{final mass remaining in capsules}}{\text{initial mass in capsules}} \times 100\% \quad (7)$$

346

347       The experimental mass median aerodynamic diameter (MMAD<sub>E</sub>) and geometric  
348 standard deviation (GSD) for the particles were determined using a Mathematica<sup>®</sup>  
349 program written by Dr. Warren Finlay (Meenach et al., 2013a; W, 2008).

350

## 351 **2.15 Statistical Analysis**

352       All measurements were performed in at least triplicate. Values are given in the  
353 form of mean ± standard deviation. The statistical significance of the results was  
354 determined using analysis of variance (ANOVA) and student's t-test. A p-value of <0.05  
355 was considered statistically significant.

356

## 357 **3. RESULTS AND DISCUSSION**

358

### 359 **3.1 Preparation and Characterization of Ac-Dex and Curcumin Nanoparticles**

360

#### 361 *3.1.1 NMR Analysis of Ac-Dex*

362       Successful synthesis of Ac-Dex was confirmed by <sup>1</sup>H NMR (**Figure S2**). Ac-Dex-  
363 5min exhibited 61.2% cyclic acetal coverage (CAC) and 71.6% total conversion of -OH

364 groups, while Ac-Dex-3h exhibited 82.5% CAC and 80.0% total conversion of -OH  
365 groups, which matched our previous results (Wang et al., 2016; Wang and Meenach,  
366 2016). The Ac-Dex with longer synthesis time (Ac-Dex-3h) exhibited a higher CAC,  
367 which was in accordance with previous studies. An increase in CAC is known to decrease  
368 polymer degradation and ultimately, the drug release rate, due to the slower degradation  
369 of the cyclic acetal groups on the Ac-Dex backbone (Bachelder et al., 2008; Broaders et  
370 al., 2009). Ac-Dex-3h also showed a higher total conversion of -OH groups, which could  
371 be a result the longer reaction time. This higher total acetal coverage is favorable in the  
372 enhancement of the stability of the PVA coating of nanoparticles (data not shown), thus  
373 ensuring small particle size and narrow size distribution.

374

### 375 *3.1.2 Dynamic Light Scattering (DLS) Analysis of Original and Redispersed CUR NP*

376 Average nanoparticle size, size distribution/polydispersion index (PDI), and zeta  
377 potential are shown in **Table 1**. No significant changes in NP size, PDI, or zeta potential  
378 was found between the original and redispersed NP ( $p < 0.05$ ), indicating that the CUR  
379 NP maintained their properties after redispersion. The original and redispersed NP  
380 exhibited an average diameter of approximately 200 nm, which is in the desirable range  
381 to avoid macrophage clearance and mucus entrapment (Kho et al., 2010). The low PDI  
382 value denotes a narrow size distribution of the NP, and the slightly negatively charged  
383 surface of nanoparticles, as measured by zeta potential, is desirable in order to reduce the  
384 interactions with negatively charged mucin fibers present in airway mucus (Lai et al.,  
385 2009). According to our preliminary experiments (data not shown), a low total  
386 conversion of -OH groups on the Ac-Dex results in NP with larger sizes and PDI due to

387 NP agglomeration. This phenomenon could be a result of the reduced hydrophobicity of  
388 Ac-Dex with fewer -OH groups converted to acetal groups, which leads to insufficient  
389 absorption of PVA on the NP surface. However, the Ac-Dex in this study was prepared to  
390 produce NP with small sizes and low PDI, as the total conversion of -OH groups was  
391 kept in a higher range to prevent NP agglomeration.

392

## 393 **3.2 Preparation and Characterization of Nanocomposite Microparticles (nCmP) and** 394 **Microparticles (MP)**

395

### 396 *3.2.1 Morphology, Sizing, and Size Distribution*

397 CUR nCmP displayed a wrinkled surface with visibly encapsulated NP as seen in  
398 **Figure 2 and Figure S3**. The raisin-like morphology of the nCmP can be attributed to  
399 the early formation of nanoparticle shells in the solution droplets during spray drying,  
400 which determines the geometric size of nCmP. As the drying process proceeds, the  
401 remaining solvent evaporates from the droplet center, resulting in hollow particles that  
402 tend to shrink (Atalar and Dervisoglu, 2015; Gu et al., 2015).

403 CUR MP were collapsed, wrinkled spheres as seen in **Figures 2D-F**. Altering the  
404 Ac-Dex composition of the particles had no impact on particle morphology. The  
405 geometric diameters ( $d_g$ ) of the CUR nCmP and MP systems are shown in **Table 2**. All of  
406 the MP  $d_g$  were approximately 1  $\mu\text{m}$  in size, which is reported to make the particles  
407 vulnerable to macrophage uptake (Sung et al., 2009). In contrast, the NP released from  
408 nCmP systems can escape macrophage clearance upon reaching the deep lung.

409

### 410 3.2.2 Analysis of Particle Density

411 The density of the particles was determined via tapped density measurements, as  
412 shown in **Table 2**. CUR nCmP exhibited tapped density values around  $0.12 \text{ g/cm}^3$ , while  
413 the MP system showed values around  $0.05 \text{ g/cm}^3$ . These density values are relatively low  
414 compared with the raw materials ( $\sim 1 \text{ g/cm}^3$ ), which can be attributed to the wrinkled  
415 morphology and hollow structures of the particle systems. It has been reported that  
416 particles  $> 1 \text{ }\mu\text{m}$  in diameter with greater density will deposit in the lungs by  
417 sedimentation (Heyder, 2004). Therefore, the increased density of CUR nCmP system as  
418 compared to MP could enhance their rate of deposition into the deep lung.

419

### 420 3.2.3 Loading and In Vitro Release of CUR

421 CUR was successfully encapsulated into both the nCmP and MP systems as seen  
422 in **Table 2**. The MP systems prepared via closed mode, organic spray drying exhibited  
423 higher encapsulation efficiency (EE,  $> 50\%$ ) than the nCmP systems (approximately  
424  $30\%$ ) prepared in open mode in aqueous solutions. The lower EE of the nCmP can be  
425 attributed to the EE of the original CUR-loaded NP, which was also approximately  $30\%$   
426 (**Table S1**). The spray drying process had no influence on the CUR loading and EE for  
427 the nCmP systems ( $p < 0.05$ ), which indicates that the drug loading of nCmP systems can  
428 be determined during NP preparation.

429 Results of the *in vitro* release of CUR from both nCmP and MP systems in  
430 modified phosphate (pH 7.4) and acetate (pH 5) buffers at physiological temperature  
431 ( $37^\circ\text{C}$ ) are reported in **Figure 3** as the percentage of cumulative drug released over time.  
432 As shown in **Table S2**, the particle systems exhibited shorter release durations and

433 increased release of CUR ( $p < 0.05$ ) at acidic pH with the exception of nCmP-5min,  
434 which only exhibited a shorter release duration. These results are in accordance with  
435 previous studies (Meenach et al., 2012; Vehring, 2008). The release profiles suggest that  
436 the drug will be released at significantly higher rates once the carrier particles reach an  
437 acidic environment. This can allow Ac-Dex particles the ability to provide controlled  
438 release of a therapeutic payload in cells and tissue with lower pH values, such as tumor  
439 cells and macrophages. In contrast, if the carrier particles remain in the extracellular or  
440 neutral pH environments, the release rate can be reduced, which can minimize systemic  
441 and local cytotoxicity (Meenach et al., 2012).

442 In addition, the nCmP systems exhibited faster release than the MP systems,  
443 which is likely due to the larger surface area available in the nano-sized delivery systems.  
444 Upon reaching an aqueous environment, the nCmP dissociate into nanoparticles with  
445 large surface areas and a PVA coating that facilitates particle dispersity, while the MP  
446 may agglomerate due to their highly hydrophobic, uncoated surfaces. As a result, the  
447 nCmP systems undergo faster polymer degradation and drug diffusion, resulting in a  
448 faster release of payloads than MP at both acidic and physiologic pH.

449 Particles comprised of Ac-Dex-3h exhibited slower release rates than those  
450 comprised of Ac-Dex-5min, indicating that the drug release rate can be controlled by the  
451 polymer reaction time. At pH 7.4, particles made of Ac-Dex-h exhibited a drug release  
452 rate between Ac-Dex-5 min and Ac-Dex-3h, suggesting that the ratio of different types of  
453 Ac-Dex can also act as an important factor in adjusting the release profiles of particle  
454 systems. Nevertheless, the drug release rates of the Ac-Dex particles at pH 5 did not  
455 follow this trend, which could be explained by one of the following: (1) the release

456 profile of Ac-Dex particles is polymer degradation controlled and the decomposition of  
457 the Ac-Dex matrix is greatly impacted by the release buffer pH and (2) the release profile  
458 of Ac-Dex particles is both polymer degradation and drug diffusion controlled. In  
459 previous studies, drug release from Ac-Dex particles was associated with Ac-Dex  
460 degradation (Bachelder et al., 2008; Kauffman et al., 2012; Meenach et al., 2012).  
461 However, Ac-Dex degradation may result in the surface erosion of particles, formation of  
462 large pores in the particles that facilitate drug diffusion, or both at the same time. As a  
463 result, the drug release profile could be controlled by drug diffusion through water-filled  
464 pores (diffusion controlled), polymer erosion on the particle surface (erosion controlled),  
465 or both drug diffusion and surface erosion (diffusion and erosion controlled), respectively  
466 (Broaders et al., 2009).

467 In order to further illustrate the mechanism of drug release of Ac-Dex particles,  
468 we fitted the CUR release data to several commonly utilized drug release models,  
469 including: (1) a first order model and (2) Hixson–Crowell model for drug dissolution-  
470 controlled release, (3) Higuchi model modified to fit burst release at time 0, (4)  
471 Korsmeyer–Peppas model and (5) Baker–Lonsdale for drug diffusion-controlled release,  
472 (6) Hopfenberg model for surface erosion-controlled release, (7) Baker’s model for both  
473 degradation and diffusion-controlled release, and (8) Weibull model as a general  
474 empirical equation to describe a dissolution or release process (Bohrey et al., 2016; Costa  
475 and Sousa Lobo, 2001; Kamaly et al., 2016; Seidlitz and Weitschies, 2012; Shuwisitkul,  
476 2011). The coefficient of determinations ( $R^2$ ) of the fit for the models are summarized in  
477 **Table S3**. The modified Higuchi and Baker–Lonsdale models exhibited higher  $R^2$   
478 compared with other models, indicating that the drug release profiles of all Ac-Dex

479 particles at both acidic and neutral pH was due primarily to drug diffusion. For Baker's  
480 model (Shuwisitkul, 2011) that describes a degradation and diffusion process, the optimal  
481 coefficient  $k$  was 0, thus the equation of Baker's model exhibited the same form as the  
482 equation for the Higuchi model. Since the degradation of Ac-Dex was observable during  
483 the release experiments, the release profiles of Ac-Dex particles can be explained by the  
484 mechanism of drug diffusion through water-filled pores (Kamaly et al., 2016). In the  
485 process of drug diffusion through water-filled pores, water was absorbed by Ac-Dex  
486 particles and filled in the pores of the polymer matrix, through which the drug diffused  
487 into the buffer. As polymer degraded, both pore size and number increased, resulting in  
488 enhanced drug release. Therefore, the reaction time of Ac-Dex affected the drug release  
489 rate significantly by controlling the formation of pores of particle matrix but not polymer  
490 degradation on the surface. Meanwhile, the water absorption into the particles may also  
491 influence the drug release rate, which can be supported by the fact that Ac-Dex-3h had a  
492 higher ratio of total hydrophobic acetalated group conversion than Ac-Dex-5min. The  
493 fitted release curves using modified Higuchi model are shown in **Figure S4** along with  
494 the original data points. The model was modified to fit the burst release at time 0 of the  
495 particle systems, which can be attributed to CUR being initially available on the surface  
496 of the particles. The nCmP systems exhibited a high release at time 0 because the  
497 nanoparticle suspension was sonicated before spray drying to form a uniform dispersion,  
498 which may cause CUR release in to the suspension.

499

#### 500 3.3.4 Karl Fischer Titration



501 The residual water content of CUR nCmP and MP is shown in **Table 2**. The water  
502 content of nCmP system was approximately 8%, while that of MP system was  
503 approximately 6%. The lower water content of MP samples is likely due to the absence of  
504 water during the closed mode spray drying process. All particle systems showed  
505 acceptable water content for aerosol formulations. In general, reducing the water content  
506 in inhalable dry powders can significantly improve their dispersion properties and  
507 enhance the stability of the powders during storage (Hickey et al., 2007; Mohammadi et  
508 al., 2010). Correspondingly, low water content in inhalable dry powders is highly  
509 favorable for efficient dry powder aerosolization and effective particle delivery  
510 (Mohammadi et al., 2010; Wu et al., 2013).

511

### 512 *3.3.5 Differential Scanning Calorimetry*

513 **Figure 4** shows DSC thermograms of the raw materials used in particle  
514 preparation and the final CUR nCmP and CUR MP systems. Both the raw Ac-Dex-5min  
515 and Ac-Dex-3h displayed endothermic phase transition peaks due to melting ( $T_m$ ) near  
516 170 °C. The peaks were broad because of the wide size distribution of Ac-Dex polymer  
517 crystallites. None of the CUR nCmP systems exhibited a peak corresponding to Ac-Dex  
518 melting, which indicates that the Ac-Dex was transformed in an amorphous state by rapid  
519 precipitation during NP formation. The CUR MP systems exhibited broad phase  
520 transition peaks near 160 °C, which corresponds to the melting of Ac-Dex. This phase  
521 transition shifted to the lower temperature range, indicating a reduction in the  
522 crystallinity of Ac-Dex after the spray drying process.

523

### 524 3.3.6 Powder X-ray Diffraction (PXRD)

525 X-ray diffraction diffractograms of the raw materials, physical mixture of Ac-Dex  
526 and CUR, CUR nCmP, and CUR MP are shown in **Figure 5**. No peaks were present for  
527 either raw Ac-Dex samples, suggesting an irregular distribution or lack of Ac-Dex  
528 crystallites. The absence of diffraction peaks from Ac-Dex is quite different from  
529 commercialized polymers such as PLGA, which exhibits strong XRD characterization  
530 peaks (Mohammadi et al., 2010). This phenomenon is likely because the Ac-Dex was  
531 collected by rapid precipitation in water, which prevents the formation of large polymer  
532 crystallites. Strong peaks were present for raw CUR indicating that it was in crystalline  
533 form prior to spray drying. XRD diffractograms of the physical mixture, CUR nCmP and  
534 CUR MP were absent of any diffraction peaks corresponding to raw CUR, which was  
535 due to the dilution effect of Ac-Dex. The results obtained from the XRD diffractograms  
536 confirmed those from DSC thermograms, which show that raw CUR was converted to  
537 amorphous forms during the particle manufacturing process.

538

### 539 3.3.7 In Vitro Aerosol Dispersion Performance Using Next Generation Impactor (NGI)

540 *In vitro* aerosol dispersion performance properties of the nCmP were evaluated  
541 using a Next Generation Impactor™ coupled with a human DPI device (**Figure 6 and**  
542 **Figure 7**). The results indicated that the formulated nCmP and MP are favorable for  
543 efficient dry powder aerosolization and effective targeted pulmonary delivery. The  
544 experimental mass mean aerodynamic diameter (MMAD<sub>E</sub>) values of all particle systems  
545 were approximately 2 μm, while the geometric standard deviation (GSD) values were 2 -  
546 3 μm. The MMAD<sub>E</sub> values were within the range of 1 - 5 μm that is required for

547 predominant deposition of particles into the deep lung region (Meenach et al., 2013b),  
548 which would be desirable to deliver therapeutics for the treatment of both local and  
549 systematic diseases through the lung. The theoretical mass mean aerodynamic diameter  
550 ( $MMAD_T$ , **Table 2**), calculated using the geometric diameter and tapped density, was  
551 lower than the experimental MMAD. This discrepancy is likely due to particle  
552 agglomeration, which increased the geometric size of the dry powder particulates. All of  
553 the particle systems exhibited low tapped density values, which supports the hypothesis  
554 that the particles are likely hollow. This can also be attributed to their wrinkled surface  
555 morphology, as seen in SEM analysis. The GSD values were within the range of those  
556 previously reported and the respirable fraction (RF), fine particle fraction (FPF), and  
557 emitted dose (ED) values were all higher than reports from similar systems (Meenach et  
558 al., 2013a; Meenach et al., 2013b; Ungaro et al., 2006). The formulated Ac-Dex particle  
559 systems are expected to achieve an improved therapeutic effect with a reduced amount of  
560 payloads by effectively delivering drugs into the deep lung region.

561

#### 562 **4. CONCLUSIONS**

563 Two types of pulmonary delivery systems were successfully formulated using Ac-  
564 Dex with two different degradation rates. The resulting CUR MP were wrinkled spheres  
565 (approximately 1  $\mu\text{m}$ ), while nCmP were similar in size with wrinkled surfaces that  
566 showed the presence of nanoparticles. The variations in the drug release rates from the  
567 Ac-Dex particles were influenced by the Ac-Dex reaction time, ratio of two types of Ac-  
568 Dex, and the particle size, which could be easily tuned during the manufacturing process.  
569 The pH value of the environment also had a significant influence on the release profiles,

570 allowing the Ac-Dex particles to release the payload in a controlled fashion. All nCmP  
571 and MP systems exhibited desirable properties as dry powder inhalation formulations,  
572 including small aerodynamic diameters, which is suitable for deep lung delivery, low  
573 water content, which is favorable for particle storage, and amorphization of a crystalline  
574 payload, which improves the efficiency of drug dissolution. Overall, the engineered Ac-  
575 Dex aerosol particle systems have the potential for targeted delivery of therapeutics into  
576 the deep lung.

577

## 578 **ACKNOWLEDGEMENTS**

579 The authors gratefully acknowledge financial support from an Institutional  
580 Development Award (IDeA) from the National Institute of General Medical Sciences of  
581 the National Institutes of Health under grant number P20GM103430. The content is  
582 solely the responsibility of the authors and does not necessarily represent the official  
583 views of the National Institutes of Health. This material is based upon work conducted at  
584 a Rhode Island NSF EPSCoR research facility, supported in part by the National Science  
585 Foundation EPSCoR Cooperative Agreement #EPS-1004057. In addition, this material is  
586 based in part upon work supported by the National Science Foundation under grant  
587 number #1508868. Any opinions, findings, and conclusions or recommendations  
588 expressed in this material are those of the authors and do not necessarily reflect the view  
589 of the National Science Foundation. Finally, the authors thank RI-INBRE for UPLC  
590 access and RIN2 for SEM, DLS, PXRD, and DSC access.

591

## 592 **AUTHOR DISCLOSURE STATEMENT**

593 No conflicts of interest exist.

594

595

596

597

598

599

## 600 REFERENCES

601 Akl, M.A., Kartal-Hodzic, A., Oksanen, T., Ismael, H.R., Afouna, M.M., Yliperttula, M.,  
602 Samy, A.M., Viitala, T., 2016. Factorial design formulation optimization and in vitro  
603 characterization of curcumin-loaded PLGA nanoparticles for colon delivery. *Journal of*  
604 *Drug Delivery Science and Technology* 32, Part A, 10-20.

605 Atalar, I., Dervisoglu, M., 2015. Optimization of spray drying process parameters for  
606 kefir powder using response surface methodology. *LWT - Food Science and Technology*  
607 60, 751-757.

608 Bachelder, E.M., Beaudette, T.T., Broaders, K.E., Dashe, J., Fréchet, J.M.J., 2008.  
609 Acetal-Derivatized Dextran: An Acid-Responsive Biodegradable Material for  
610 Therapeutic Applications. *Journal of the American Chemical Society* 130, 10494-10495.

611 Belotti, S., Rossi, A., Colombo, P., Bettini, R., Rekkas, D., Politis, S., Colombo, G.,  
612 Balducci, A.G., Buttini, F., 2015. Spray-dried amikacin sulphate powder for inhalation in  
613 cystic fibrosis patients: The role of ethanol in particle formation. *European Journal of*  
614 *Pharmaceutics and Biopharmaceutics* 93, 165-172.

615 Bohrey, S., Chourasiya, V., Pandey, A., 2016. Polymeric nanoparticles containing  
616 diazepam: preparation, optimization, characterization, in-vitro drug release and release  
617 kinetic study. *Nano Convergence* 3, 1-7.

618 Broaders, K.E., Cohen, J.A., Beaudette, T.T., Bachelder, E.M., Fréchet, J.M.J., 2009.  
619 Acetalated dextran is a chemically and biologically tunable material for particulate  
620 immunotherapy. *Proceedings of the National Academy of Sciences* 106, 5497-5502.

621 Cohen, J.A., Beaudette, T.T., Cohen, J.L., Broaders, K.E., Bachelder, E.M., Frechet,  
622 J.M., 2010. Acetal-modified dextran microparticles with controlled degradation kinetics  
623 and surface functionality for gene delivery in phagocytic and non-phagocytic cells.  
624 *Advanced materials (Deerfield Beach, Fla.)* 22, 3593-3597.

625 Collier, M.A., Peine, K.J., Gautam, S., Oghumu, S., Varikuti, S., Borteh, H., Papenfuss,  
626 T.L., Sataoskar, A.R., Bachelder, E.M., Ainslie, K.M., 2016. Host-mediated *Leishmania*  
627 *donovani* treatment using AR-12 encapsulated in acetalated dextran microparticles. *Int J*  
628 *Pharm* 499, 186-194.

629 Costa, P., Sousa Lobo, J.M., 2001. Modeling and comparison of dissolution profiles.  
630 *European Journal of Pharmaceutical Sciences* 13, 123-133.

631 Cui, L., Cohen, J.A., Broaders, K.E., Beaudette, T.T., Frechet, J.M., 2011. Mannosylated  
632 dextran nanoparticles: a pH-sensitive system engineered for immunomodulation through  
633 mannose targeting. *Bioconjugate chemistry* 22, 949-957.

634 Gu, B., Linehan, B., Tseng, Y.-C., 2015. Optimization of the Büchi B-90 spray drying  
635 process using central composite design for preparation of solid dispersions. *International*  
636 *Journal of Pharmaceutics* 491, 208-217.

637 He, C., Hu, Y., Yin, L., Tang, C., Yin, C., 2010. Effects of particle size and surface  
638 charge on cellular uptake and biodistribution of polymeric nanoparticles. *Biomaterials* 31,  
639 3657-3666.

640 Heyder, J., 2004. Deposition of Inhaled Particles in the Human Respiratory Tract and  
641 Consequences for Regional Targeting in Respiratory Drug Delivery. *Proceedings of the*  
642 *American Thoracic Society* 1, 315-320.

643 Hickey, A.J., Mansour, H.M., Telko, M.J., Xu, Z., Smyth, H.D., Mulder, T., McLean, R.,  
644 Langridge, J., Papadopoulos, D., 2007. Physical characterization of component particles  
645 included in dry powder inhalers. I. Strategy review and static characteristics. *J Pharm Sci*  
646 96, 1282-1301.

647 Hoang, K.V., Borteh, H.M., Rajaram, M.V., Peine, K.J., Curry, H., Collier, M.A.,  
648 Homsy, M.L., Bachelder, E.M., Gunn, J.S., Schlesinger, L.S., Ainslie, K.M., 2014.  
649 Acetalated dextran encapsulated AR-12 as a host-directed therapy to control *Salmonella*  
650 infection. *Int J Pharm* 477, 334-343.

651 Jensen, D.M., Cun, D., Maltesen, M.J., Frokjaer, S., Nielsen, H.M., Foged, C., 2010.  
652 Spray drying of siRNA-containing PLGA nanoparticles intended for inhalation. *Journal*  
653 *of controlled release : official journal of the Controlled Release Society* 142, 138-145.

654 Kamaly, N., Yameen, B., Wu, J., Farokhzad, O.C., 2016. Degradable Controlled-Release  
655 Polymers and Polymeric Nanoparticles: Mechanisms of Controlling Drug Release.  
656 *Chemical Reviews* 116, 2602-2663.

657 Kanthamneni, N., Sharma, S., Meenach, S.A., Billet, B., Zhao, J.-C., Bachelder, E.M.,  
658 Ainslie, K.M., 2012. Enhanced stability of horseradish peroxidase encapsulated in  
659 acetalated dextran microparticles stored outside cold chain conditions. *International*  
660 *Journal of Pharmaceutics* 431, 101-110.

661 Kauffman, K.J., Kanthamneni, N., Meenach, S.A., Pierson, B.C., Bachelder, E.M.,  
662 Ainslie, K.M., 2012. Optimization of rapamycin-loaded acetalated dextran microparticles  
663 for immunosuppression. *International Journal of Pharmaceutics* 422, 356-363.

664 Kho, K., Cheow, W.S., Lie, R.H., Hadinoto, K., 2010. Aqueous re-dispersibility of spray-  
665 dried antibiotic-loaded polycaprolactone nanoparticle aggregates for inhaled anti-biofilm  
666 therapy. *Powder Technology* 203, 432-439.

667 Lai, S.K., Wang, Y.-Y., Hanes, J., 2009. Mucus-penetrating nanoparticles for drug and  
668 gene delivery to mucosal tissues. *Advanced drug delivery reviews* 61, 158-171.

669 Mansour, H.M., Rhee, Y.-S., Wu, X., 2009. Nanomedicine in pulmonary delivery.  
670 *International journal of nanomedicine* 4, 299-319.

671 Meenach, S.A., Anderson, K.W., Zach Hilt, J., McGarry, R.C., Mansour, H.M., 2013a.  
672 Characterization and aerosol dispersion performance of advanced spray-dried  
673 chemotherapeutic PEGylated phospholipid particles for dry powder inhalation delivery in  
674 lung cancer. *European Journal of Pharmaceutical Sciences* 49, 699-711.

675 Meenach, S.A., Kim, Y.J., Kauffman, K.J., Kanthamneni, N., Bachelder, E.M., Ainslie,  
676 K.M., 2012. Synthesis, Optimization, and Characterization of Camptothecin-Loaded  
677 Acetalated Dextran Porous Microparticles for Pulmonary Delivery. *Molecular*  
678 *Pharmaceutics* 9, 290-298.

679 Meenach, S.A., Vogt, F.G., Anderson, K.W., Hilt, J.Z., McGarry, R.C., Mansour, H.M.,  
680 2013b. Design, physicochemical characterization, and optimization of organic solution  
681 advanced spray-dried inhalable dipalmitoylphosphatidylcholine (DPPC) and  
682 dipalmitoylphosphatidylethanolamine poly(ethylene glycol) (DPPE-PEG) microparticles

683 and nanoparticles for targeted respiratory nanomedicine delivery as dry powder  
684 inhalation aerosols. *International journal of nanomedicine* 8, 275-293.

685 Mohammadi, G., Valizadeh, H., Barzegar-Jalali, M., Lotfipour, F., Adibkia, K., Milani,  
686 M., Azhdarzadeh, M., Kiafar, F., Nokhodchi, A., 2010. Development of azithromycin-  
687 PLGA nanoparticles: physicochemical characterization and antibacterial effect against  
688 *Salmonella typhi*. *Colloids and surfaces. B, Biointerfaces* 80, 34-39.

689 Rasband, W.S., 1997-2016. ImageJ.

690 Seidlitz, A., Weitschies, W., 2012. In-vitro dissolution methods for controlled release  
691 parenterals and their applicability to drug-eluting stent testing. *The Journal of pharmacy  
692 and pharmacology* 64, 969-985.

693 Shuwisitkul, D., 2011. title., Freie Universität Berlin.

694 Sung, J.C., Padilla, D.J., Garcia-Contreras, L., Verberkmoes, J.L., Durbin, D., Peloquin,  
695 C.A., Elbert, K.J., Hickey, A.J., Edwards, D.A., 2009. Formulation and pharmacokinetics  
696 of self-assembled rifampicin nanoparticle systems for pulmonary delivery. *Pharm Res* 26,  
697 1847-1855.

698 Takashima, Y., Saito, R., Nakajima, A., Oda, M., Kimura, A., Kanazawa, T., Okada, H.,  
699 2007. Spray-drying preparation of microparticles containing cationic PLGA nanospheres  
700 as gene carriers for avoiding aggregation of nanospheres. *Int J Pharm* 343, 262-269.

701 Tomoda, K., Ohkoshi, T., Kawai, Y., Nishiwaki, M., Nakajima, T., Makino, K., 2008.  
702 Preparation and properties of inhalable nanocomposite particles: effects of the  
703 temperature at a spray-dryer inlet upon the properties of particles. *Colloids and surfaces.  
704 B, Biointerfaces* 61, 138-144.

705 Ulery, B.D., Nair, L.S., Laurencin, C.T., 2011. Biomedical Applications of  
706 Biodegradable Polymers. *Journal of polymer science. Part B, Polymer physics* 49, 832-  
707 864.

708 Ungaro, F., De Rosa, G., Miro, A., Quaglia, F., La Rotonda, M.I., 2006. Cyclodextrins in  
709 the production of large porous particles: Development of dry powders for the sustained  
710 release of insulin to the lungs. *European Journal of Pharmaceutical Sciences* 28, 423-432.

711 Vehring, R., 2008. Pharmaceutical Particle Engineering via Spray Drying. *Pharm Res* 25,  
712 999-1022.

713 W, F., 2008. The ARLA Respiratory Deposition Calculator.

714 Wang, Z., Cuddigan, J.L., Gupta, S.K., Meenach, S.A., 2016. Nanocomposite  
715 Microparticles (nCmP) for the Delivery of Tacrolimus in the Treatment of Pulmonary  
716 Arterial Hypertension. *International Journal of Pharmaceutics* 512, 305-313.

717 Wang, Z., Meenach, S.A., 2016. Synthesis and Characterization of Nanocomposite  
718 Microparticles (nCmP) for the Treatment of Cystic Fibrosis-Related Infections.  
719 *Pharmaceutical Research* 33, 1862-1872.

720 Wu, L., Miao, X., Shan, Z., Huang, Y., Li, L., Pan, X., Yao, Q., Li, G., Wu, C., 2014.  
721 Studies on the spray dried lactose as carrier for dry powder inhalation. *Asian Journal of  
722 Pharmaceutical Sciences* 9, 336-341.

723 Wu, X., Zhang, W., Hayes, D., Jr., Mansour, H.M., 2013. Physicochemical  
724 characterization and aerosol dispersion performance of organic solution advanced spray-  
725 dried cyclosporine A multifunctional particles for dry powder inhalation aerosol delivery.  
726 *Int J Nanomedicine* 8, 1269-1283.

727

728

729 **TABLES AND FIGURES**

730

731 **Table 1.** Average diameter (as measured by dynamic light scattering), polydispersity  
 732 index (PDI), and zeta potential (ZP) of CUR-loaded nanoparticles before spray drying  
 733 (NP) and after redispersion from nanocomposite microparticles (nCmP) (mean  $\pm$  standard  
 734 deviation,  $n = 3$ ).

735

Particle System	Average Diameter (nm)	PDI	ZP (mV)
NP-5min	192.2 $\pm$ 2.7	0.07 $\pm$ 0.03	-8.4 $\pm$ 4.1
NP-h	201.1 $\pm$ 1.5	0.02 $\pm$ 0.01	-8.0 $\pm$ 3.7
NP-3h	206.1 $\pm$ 1.3	0.03 $\pm$ 0.03	-7.0 $\pm$ 1.6
nCmP-5min	199.3 $\pm$ 1.3	0.09 $\pm$ 0.02	-14.5 $\pm$ 1.0
nCmP-h	210.2 $\pm$ 2.5	0.07 $\pm$ 0.01	-13.3 $\pm$ 1.9
nCmP-3h	213.5 $\pm$ 2.4	0.02 $\pm$ 0.00	-11.2 $\pm$ 1.6

736

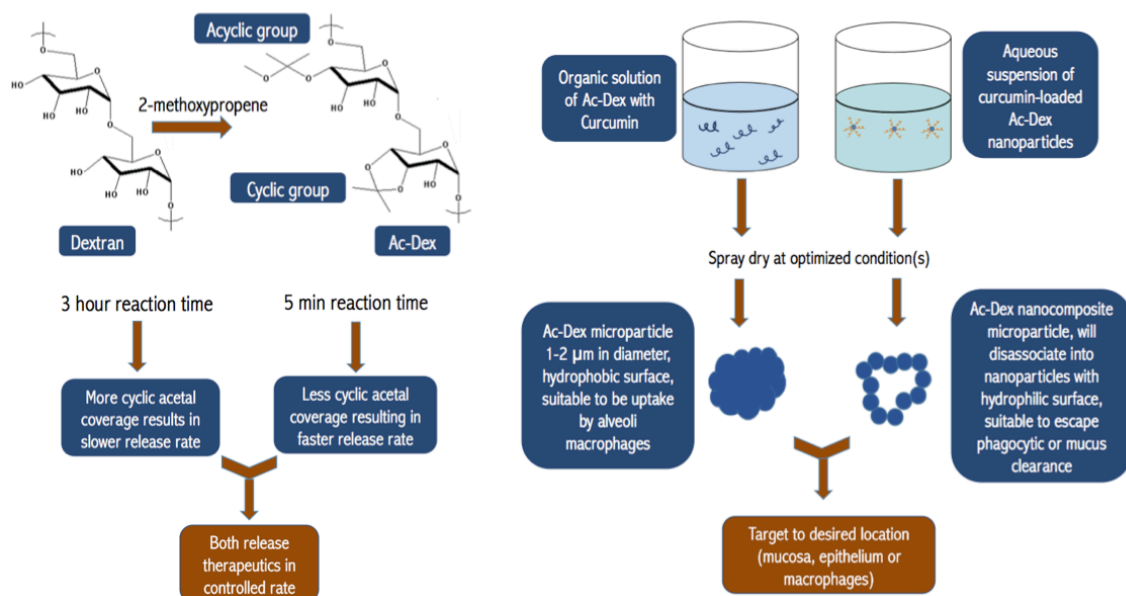
737 **Table 2.** Geometric diameter (as measured by SEM imaging and ImageJ analysis),  
 738 experimental mass median aerodynamic diameter (MMAD<sub>E</sub>), geometric standard  
 739 deviation (GSD), water content, tapped density, theoretical mean mass aerodynamic  
 740 diameter (MMAD<sub>T</sub>), drug loading, and drug encapsulation efficiency (EE) of nCmP and  
 741 MP (mean  $\pm$  standard deviation,  $n = 3$ ).

Particle System	Geometric Diameter ( $\mu\text{m}$ )	MMAD <sub>E</sub> ( $\mu\text{m}$ )	GSD ( $\mu\text{m}$ )	Water Content (%)	Tapped Density ( $\text{g}/\text{cm}^3$ )	MMAD <sub>T</sub> ( $\mu\text{m}$ )	Drug Loading (mg/100 mg particle)	EE (%)
nCmP-5min	1.52 $\pm$ 0.33	1.61 $\pm$ 0.16	2.37 $\pm$ 0.24	7.69 $\pm$ 0.76	0.122 $\pm$ 0.001	0.52 $\pm$ 0.09	0.57 $\pm$ 0.006	28.7 $\pm$ 0.32
nCmP-h	1.77 $\pm$ 0.46	2.05 $\pm$ 0.09	2.62 $\pm$ 0.17	7.89 $\pm$ 1.56	0.115 $\pm$ 0.004	0.60 $\pm$ 0.09	0.58 $\pm$ 0.008	28.4 $\pm$ 0.42
nCmP-3h	1.72 $\pm$ 0.39	1.89 $\pm$ 0.09	2.70 $\pm$ 0.13	7.86 $\pm$ 0.43	0.133 $\pm$ 0.002	0.64 $\pm$ 0.12	0.62 $\pm$ 0.013	31.2 $\pm$ 0.63
MP-5min	0.89 $\pm$ 0.30	2.38 $\pm$ 0.06	2.14 $\pm$ 0.14	6.12 $\pm$ 1.33	0.050 $\pm$ 0.001	0.21 $\pm$ 0.03	1.33 $\pm$ 0.092	66.3 $\pm$ 4.62
MP-h	1.26 $\pm$ 0.41	2.21 $\pm$ 0.23	2.17 $\pm$ 0.03	5.87 $\pm$ 1.85	0.050 $\pm$ 0.001	0.29 $\pm$ 0.32	1.03 $\pm$ 0.030	51.6 $\pm$ 1.48
MP-3h	1.05 $\pm$ 0.36	2.41 $\pm$ 0.07	2.02 $\pm$ 0.08	5.23 $\pm$ 1.13	0.052 $\pm$ 0.001	0.23 $\pm$ 0.03	1.12 $\pm$ 0.012	55.8 $\pm$ 0.61

742



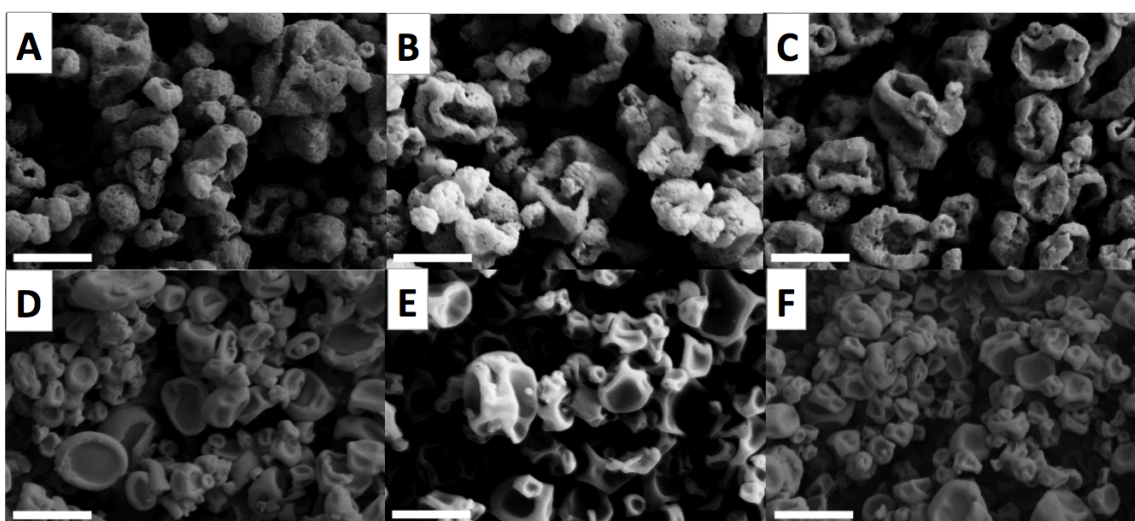
743



744

745 **Figure 1.** Schematic depicting the synthesis of Ac-Dex (Left) and preparation of  
746 nanoparticles and formation of nanocomposite microparticles (nCmP) and microparticles  
747 (MP) (Right).

748

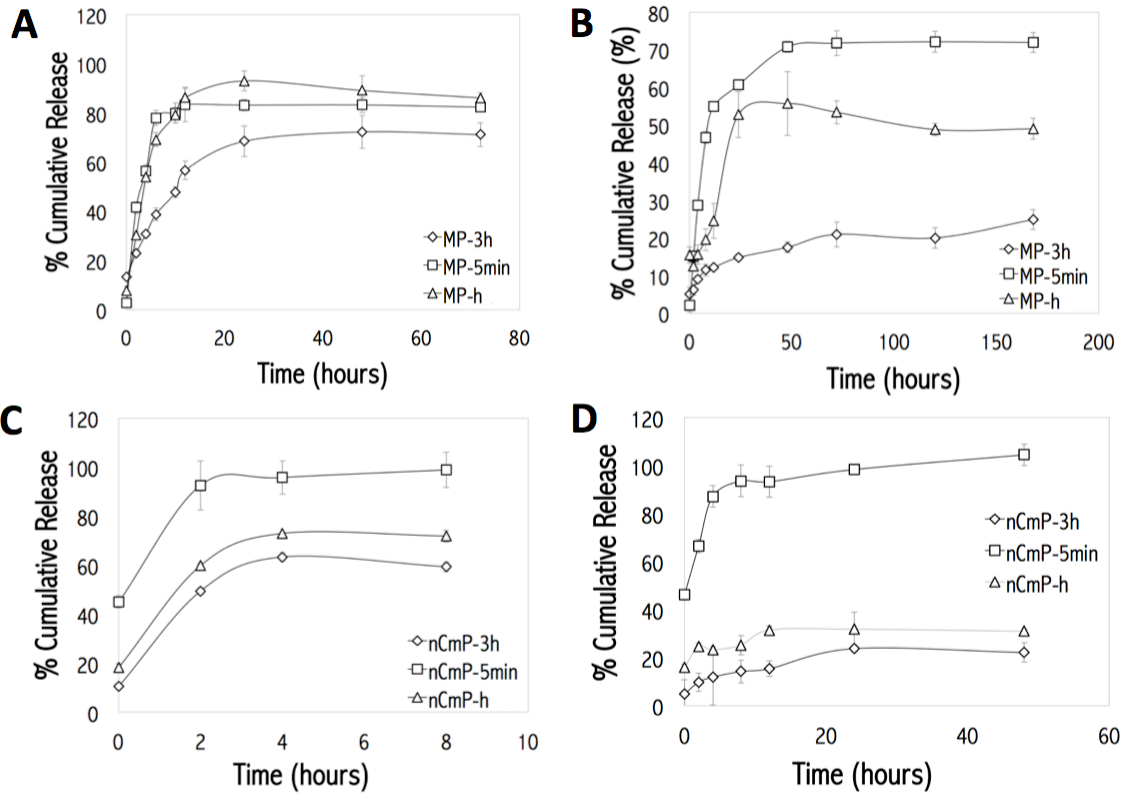


749

750 **Figure 2.** SEM micrographs of curcumin-loaded nanocomposite microparticles (CUR  
751 nCmP) and microparticles (CUR MP) including: (A) CUR nCmP-5min, (B) CUR nCmP-  
752 h, (C) CUR nCmP-3h, (D) CUR MP-5min, (E) CUR MP-h, and (F) CUR MP-3h  
753 systems. Scale bar = 2 μm.

754

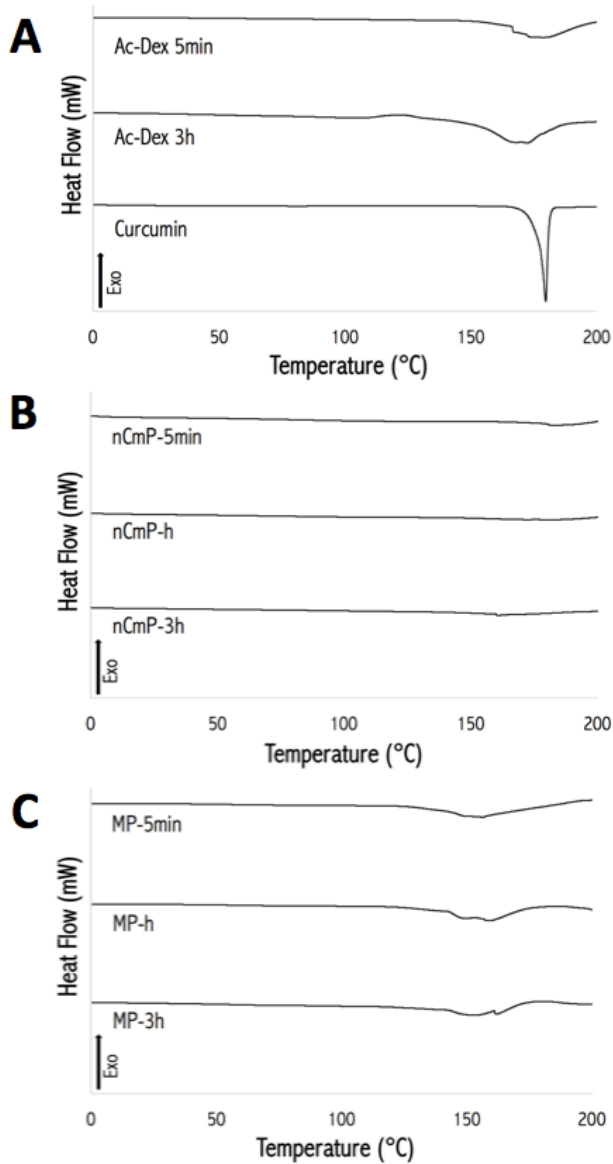
755



756

757 **Figure 3.** *In vitro* drug release profiles for curcumin-loaded microparticle (MP) systems  
758 at (A) pH 5 and (B) pH 7.4 and curcumin-loaded nanocomposite microparticle (nCmP)  
759 system at (C) pH 5 and (D) pH 7.4.

760

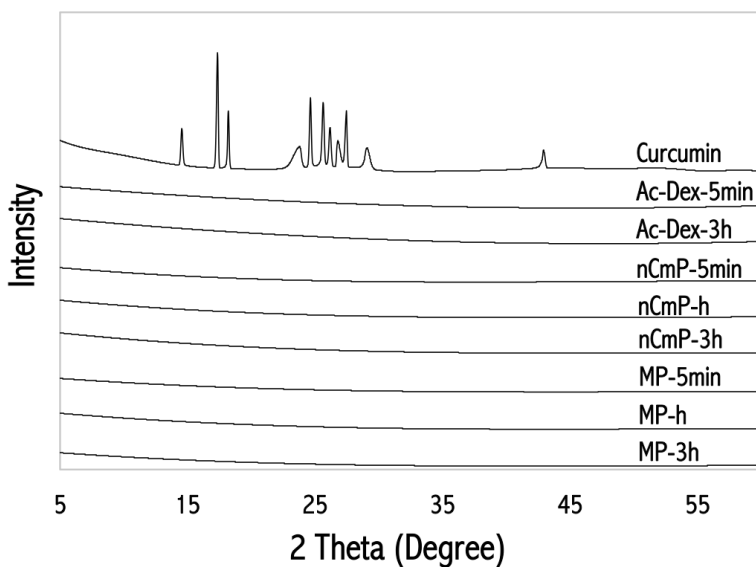


761

762 **Figure 4.** Representative differential scanning calorimetry (DSC) thermograms of (A)  
 763 raw curcumin (CUR), raw acetalated dextran-5min (Ac-Dex-5min), and raw acetalated  
 764 dextran-3h (Ac-Dex-3h), (B) CUR nCmP-5min, CUR nCmP-h, and CUR nCmP-3h, and  
 765 (C) CUR MP-5min, CUR MP-h, and CUR MP-3h.

766

767

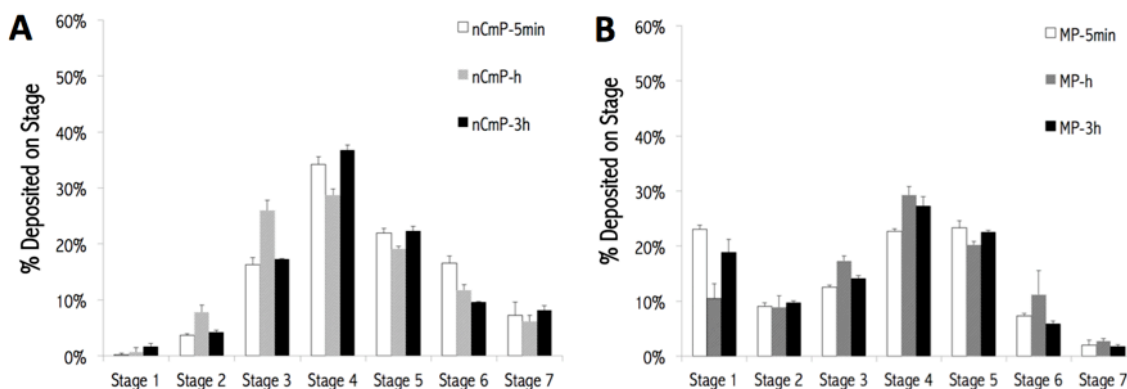


768

769 **Figure 5.** Representative powder X-ray diffractograms (PXRD) of raw curcumin (CUR),  
 770 raw acetalated dextran-5min (Ac-Dex-5min), raw acetalated dextran-3h (Ac-Dex-3h),  
 771 CUR nCmP-5min, CUR nCmP-h, CUR nCmP-3h, CUR MP-5min, CUR MP-h, and CUR  
 772 MP-3h.

773

774



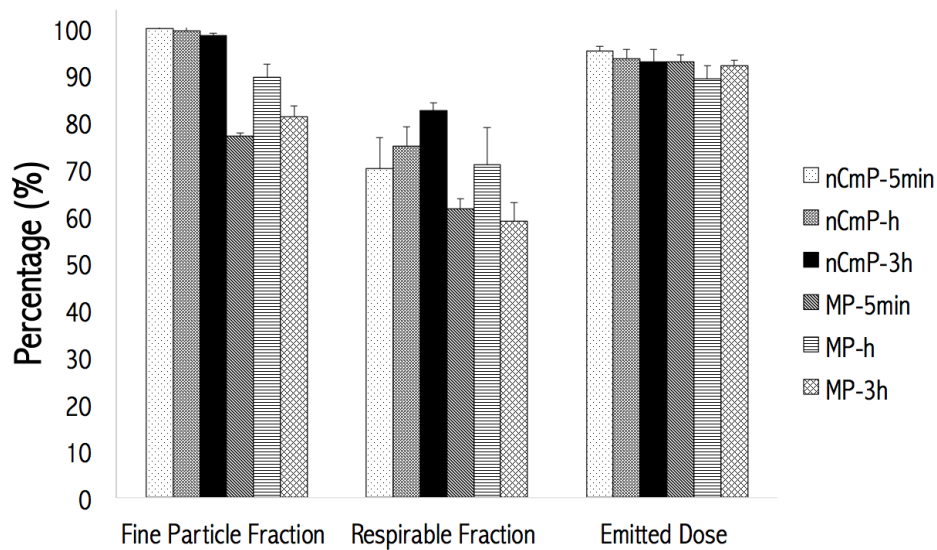
775

776 **Figure 6.** Aerosol dispersion performance of (A) curcumin-loaded nanocomposite  
 777 microparticles (CUR nCmP) and (B) microparticles (CUR MP) as % particles deposited  
 778 on each stage of the Next Generation Impactor™ (NGI™). For Q = 60 L/min, the  
 779 effective cutoff diameters ( $D_{50}$ ) for each impaction stage are as follows: stage 1 (8.06  
 780  $\mu\text{m}$ ), stage 2 (4.46  $\mu\text{m}$ ), stage 3 (2.82  $\mu\text{m}$ ), stage 4 (1.66  $\mu\text{m}$ ), stage 5 (0.94  $\mu\text{m}$ ), stage 6  
 781 (0.55  $\mu\text{m}$ ), and stage 7 (0.34  $\mu\text{m}$ ) (mean  $\pm$  standard deviation, n = 3).

782

783

784



785

786 **Figure 7.** *In vitro* aerosol dispersion performance properties including fine particle dose  
787 (FPD), fine particle fraction (FPF), respirable fraction (RF), and emitted dose (ED) for  
788 curcumin loaded nanocomposite microparticles (CUR nCmP) and microparticles (CUR  
789 MP) (mean  $\pm$  standard deviation, n = 3).

790

791

792

793

794

795

796

797

798

799

800

801

802

803

804

805

806 **SUPPLEMENTAL INFORMATION**

807

808 **S.1 Drug Release Model Descriptions**

809 The drug release data of the particle systems was fitted to several relevant models  
810 (equations shown below) to aid in the determination of the type of release the systems  
811 underwent. For the models that can be linearized (all except for Baker's model), the  
812 coefficient of determination ( $R^2$ ) was calculated to determine the applicability of the  
813 release models. For Baker's model, Microsoft Excel with Solver add-in was applied to  
814 determine the parameters that minimize the sum of squares of the residues of the model.  
815 The models, equations, and their corresponding parameters are as follows:

816

817 First order model: 
$$\log M_t = \log M_0 + \frac{K}{2.303} t \quad (S1)$$

818

819 where  $M_t$  is the amount of drug released at time  $t$ ,  $M_0$  is the initial amount of drug in the  
820 solution, and  $K$  is the first order release constant.

821

822 Weibull model: 
$$m = 1 - \exp\left(\frac{-(t - T_i)^b}{a}\right) \quad (S2)$$

823

824 where  $m$  is the accumulated fraction of the drug released at time  $t$ ,  $a$  is the scale  
825 parameter, which defines the time scale of the process,  $T_i$  is the location parameter, which  
826 represents the lag time before the onset of the dissolution or release process, and  $b$  is the  
827 shape parameter, which characterizes the shape of release curve.

828

829 Higuchi model:  $M_t = Kt^{1/2} + b$  (S3)

830

831 where  $M_t$  is the amount of drug released at time  $t$ ,  $K$  is the Higuchi dissolution constant,  
832 and  $b$  is the amount of drug released at time 0.

833

834 Hixson–Crowell model:  $W_0^{1/3} - W_t^{1/3} = Kt$  (S4)

835

836 where  $W_0$  is the initial amount of drug in the particles,  $W_t$  is the remaining amount of  
837 drug in the particles at time  $t$ , and  $K$  is a constant characterizing the surface to volume  
838 relationship.

839

840 Korsmeyer–Peppas model:  $m = at^n$  (S5)

841

842 where  $a$  is a constant characterizing the structural and geometric properties of the  
843 particles,  $n$  is the release exponent, indicating the drug release mechanism, and  $m$  is the  
844 accumulated fraction of the drug released at time  $t$ .

845

846 Baker–Lonsdale model:  $\frac{3}{2}[1 - (1 - m)^{2/3}] - m = Kt$  (S6)

847

848 where  $K$  is the release constant and  $m$  is the accumulated fraction of the drug released at  
849 time  $t$ .

850

851 Hopfenberg model:  $m = 1 - [1 - Kt(t-1)]^n$  (S7)

852

853 where  $K$  is a constant equal to  $k_0/C_0a_0$ , where  $k_0$  is the erosion rate constant,  $C_0$  is the  
854 initial concentration of drug in the matrix, and  $a_0$  is the initial radius for particles.  $m$  is the  
855 accumulated fraction of the drug released at time  $t$ .

856

857 Baker's model:  $M_t = A(2P_0e^{kt}C_0t)^{1/2}$  (S8)

858

859 where  $M_t$  is the amount of drug released in time  $t$ ,  $P_0$  is the drug permeability,  $A$  is the  
860 total area of the particle,  $C_0$  is the drug concentration at the initial time, and  $k$  is the first-  
861 order rate constant of bond cleavage of the polymer carrier.

862

863

864

865

866

867



868

869 **Table S1.** Drug loading and encapsulation efficiency of curcumin NP including NP-  
870 5min, NP-h, and NP-3h.

<b>Particle System</b>	<b>Drug Loading (mg/100mg particle)</b>	<b>EE (%)</b>
NP-5min	0.600 ± 0.059	30.0 ± 2.95
NP-h	0.621 ± 0.056	31.0 ± 2.82
NP-3h	0.617 ± 0.063	30.9 ± 3.15

871

872 **Table S2.** The release duration and total fraction of curcumin released from each particle  
873 system at acidic and neutral pH.

<b>Particle System</b>	<b>pH = 5</b>		<b>pH = 7.4</b>	
	<b>Release Duration (h)</b>	<b>Total Released (%)</b>	<b>Release Duration (h)</b>	<b>Total Released (%)</b>
nCmP-5min	2	92.6	8	93.6
nCmP-h	2	63.4	12	31.5
nCmP-3h	4	73.0	24	23.7
MP-5min	6	78.0	24	60.6
MP-h	12	86.4	24	52.7
MP-3h	24	68.5	168	24.9

874

875

876

877

878

879

880

881

882

883 **Table S3.** Summary of the coefficient of determinations ( $R^2$ ) of all the fitted drug release  
 884 models for all particle system. The model with relatively high  $R^2$  for all particle systems  
 885 was regarded as a viable fit for that system.

pH = 5						
Model	nCmP - 5min	nCmP - -h	nCmP - -3h	MP - 5min	MP -h	MP -3h
<b>First order</b>	0.7835	0.8549	0.8511	0.5730	0.4848	0.7517
<b>Hixson- Crowell</b>	0.8615	0.9571	0.9613	0.8470	0.8899	0.9490
<b>Higuchi (modified)</b>	0.9468	0.9968	0.9989	0.9867	0.9748	0.9715
<b>Korsmeyer- Peppas</b>	0.9998	0.6906	0.5050	0.8100	0.8843	0.9882
<b>Baker- Lonsdale</b>	0.8729	0.9945	0.9799	0.9065	0.9595	0.9753
<b>Hopfenberg</b>	0.5497	0.8743	0.9029	0.8925	0.849	0.9276
<b>Weibull</b>	0.9098	0.5773	0.2538	0.9387	0.9936	0.9353

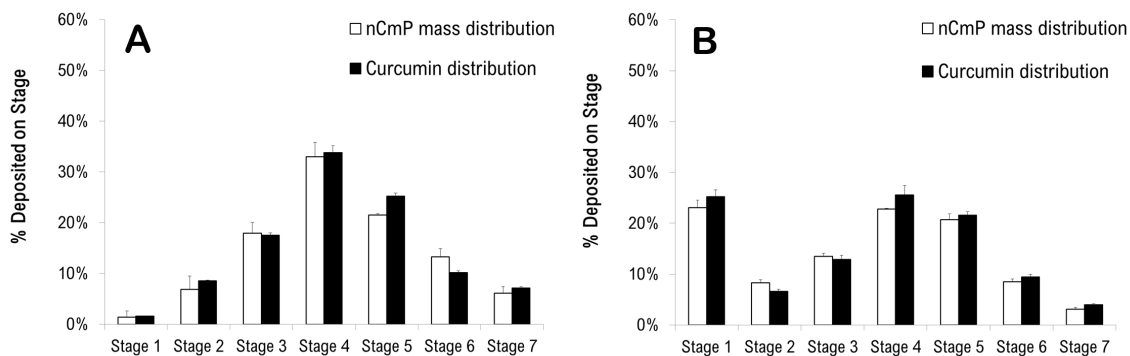
886

pH = 7.4						
Model	nCmP - 5min	nCmP - -h	nCmP - 3h	MP - 5min	MP -h	MP -3h
<b>First order</b>	0.8084	0.7345	0.7574	0.3797	0.8290	0.6414
<b>Hixson- Crowell</b>	0.9312	0.8021	0.9482	0.7696	0.9117	0.8188
<b>Higuchi (modified)</b>	0.9573	0.8758	0.9732	0.9369	0.8288	0.9462
<b>Korsmeyer- Peppas</b>	0.8990	0.5374	0.9457	0.8828	0.9349	0.9708
<b>Baker- Lonsdale</b>	0.9709	0.8172	0.9089	0.9283	0.9141	0.9074
<b>Hopfenberg</b>	0.8493	0.8678	0.9685	0.7462	0.8241	0.8526
<b>Weibull</b>	1.0000	0.5235	0.7905	0.9783	0.8897	0.8963

898

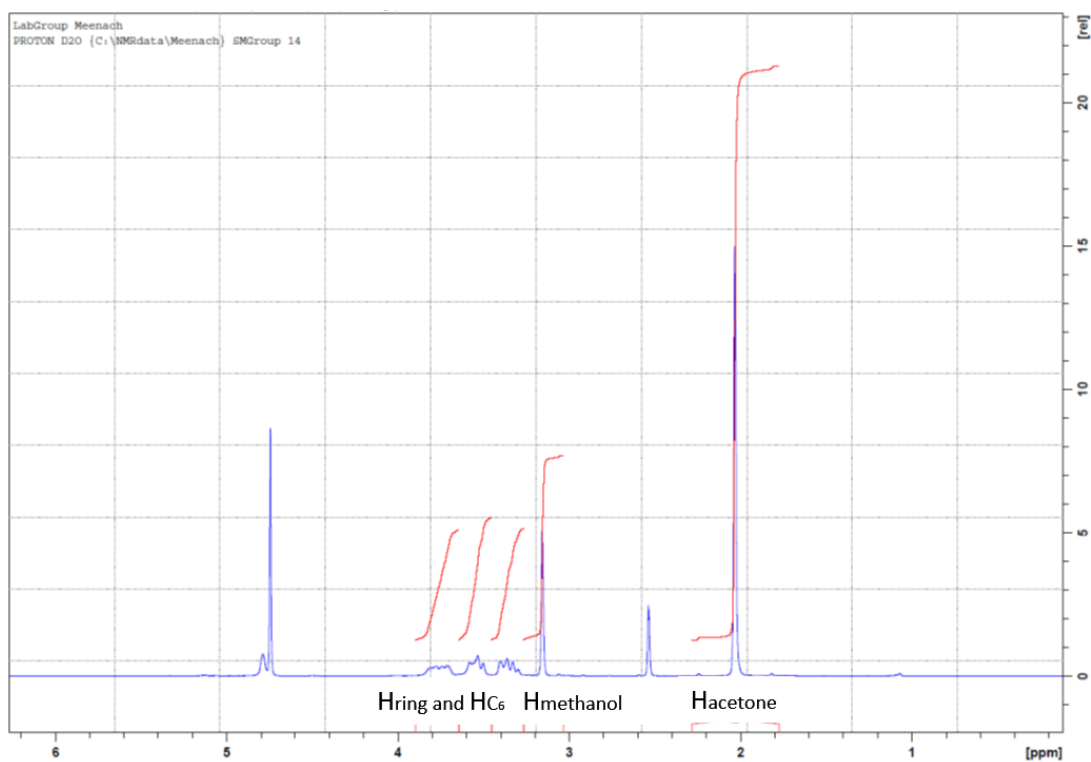
899

900



901  
902  
903  
904  
905  
906

**Figure S1.** Relationship between particle mass distribution and curcumin (CUR) distribution in all chambers of NGI for (A) CUR-nCmP and (B) CUR-MP.



907  
908  
909  
910  
911

**Figure S2.** NMR analysis of Ac-Dex where peaks using during analysis include 3.4-4.0 ppm for dextran ( $H_{ring}$  and  $H_{C_6}$ ), 3.36 ppm for methanol, and 2.08 ppm for acetone.

Cyclic acetal coverage (CAC) and total conversion of -OH group were calculated by the following equations:

$$\text{Normalization factor (NF)} = \frac{\text{Total area of 3 dextran peaks}}{6}$$

$$\text{Methanol per glucose} = \frac{\text{Methanol Peak Area}}{3 \times \text{NF}}$$

912

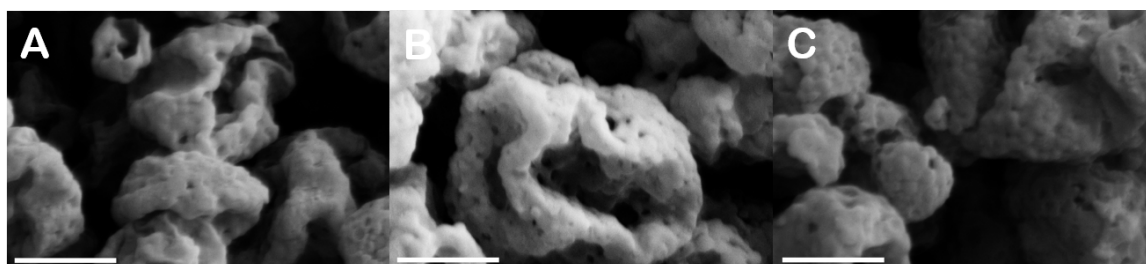
$$\text{Acetone per glucose} = \frac{\text{Acetone Peak Area}}{6 \times \text{NF}}$$

$$\text{Cyclic acetal coverage (CAC)} = (\text{Acetone per glucose} - \text{Methanol per glucose}) \times 100\%$$

$$\text{Total conversion of } -\text{OH groups} = \frac{(2 \times \text{Acetone per glucose} - \text{Methanol per glucose})}{3} \times 100\%$$

913

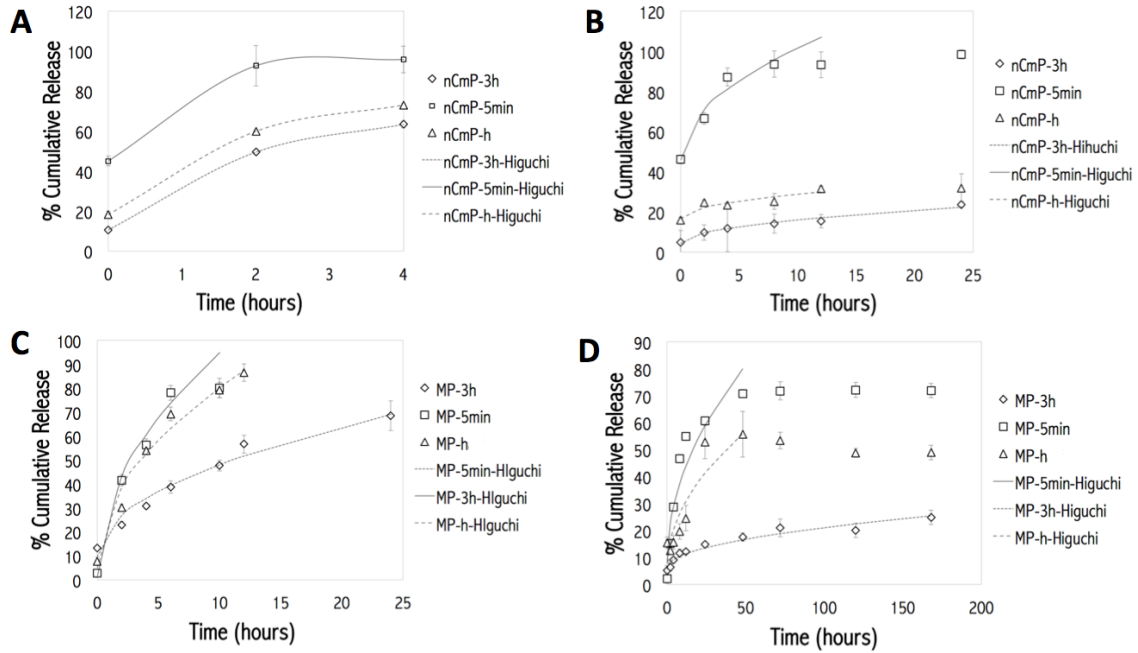
914



915

916 **Figure S3.** Zoomed in images of CUR-nCmP including: (A) CUR nCmP-5min, (B) CUR  
917 nCmP-h, (C) CUR nCmP-3h. Scale bar = 2  $\mu\text{m}$ .

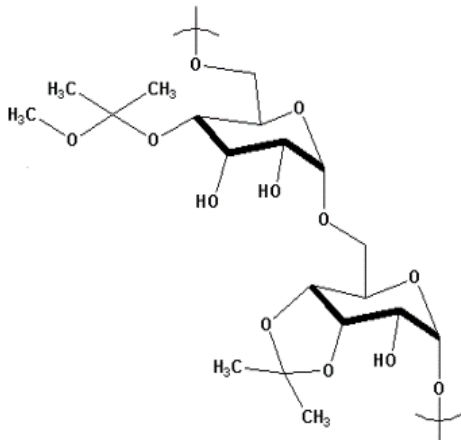
918



919

920 **Figure S4.** Original data and fitted curves of *in vitro* drug release profiles for curcumin  
 921 (CUR) nCmP (A and B) and MP systems (C and D) including CUR nCmP-5min, CUR  
 922 nCmP-h, CUR nCmP-3h, CUR MP-5min, CUR MP-h, and CUR MP-3h at pH = 5 (A and  
 923 C) and pH = 7.4 (B and D).

924



925

926 **Figure S5.** Structure of acetalated dextran (Ac-Dex).

927

928

929